Atmospheric Research 174–175 (2016) 41–51

Contents lists available at ScienceDirect

Atmospheric Research

journal homepage: www.elsevier.com/locate/atmosres

Raindrop size distribution of easterly and westerly monsoon precipitation observed over Palau islands in the Western Pacific Ocean

U.V. Murali Krishna [a], K. Krishna Reddy [a,*], Balaji Kumar Seela [b,c], Ryuichi Shirooka [d], Pay-Liam Lin [e], Chen-Jeih Pan [f]

[a] Department of Physics, Yogi Vemana University, Kadapa, Andhra Pradesh, India
[b] Taiwan International Graduate Program (TIGP), Earth System Science Program, Research Center for Environmental Changes (RCEC), Academia Sinica, Taipei, Taiwan
[c] Institute of Atmospheric Science, College of Earth Science, National Central University, Zhongli City, Taiwan
[d] Department of Coupled Ocean-Atmosphere-Land Processes Research, Japan Agency for Marine-Earth Science and Technology, Yokosuka, Japan
[e] Institute of Atmospheric Science, National Central University, Zhongli City, Taiwan
[f] Institute of Space Science, National Central University, Zhongli City, Taiwan

ARTICLE INFO

Article history:
Received 4 July 2015
Received in revised form 20 January 2016
Accepted 25 January 2016
Available online 3 February 2016

Keywords:
Raindrop size distribution (RSD)
Rainrate
Mass-weighted mean diameter
Normalized intercept parameter

ABSTRACT

This paper explores the characteristics of raindrop spectra in terms of raindrop size distribution (RSD) using 4 years of Joss–Waldvogel disdrometer data over Palau islands (7° 20′ N, 134° 28′ E) in Western Tropical Pacific ocean. The RSD characteristics are studied in two seasons (easterly monsoon—EM and westerly monsoon—WM) using three (stratiform, deep convection, and shallow convection) rain types identified from collocated 1290-MHz wind profiler radar (WPR). In addition to the ground-based sensors observations, TRMM and MODIS satellite-derived rain parameters and atmospheric parameters are utilized to study RSD characteristics. RSD characteristics stratified on the basis of rainrate show that the mean values of raindrop concentrations of small (medium and larger) drops are same (more) in WM compared to EM season. Normalized gamma distribution of RSD shows that the mean value of mass-weighted mean diameter, D_m (normalized intercept parameter, $\log_{10}N_w$), is higher (lower) in WM than the EM season. In addition, the mean value of D_m ($\log_{10}N_w$) is higher (lower) in deep convective precipitation as compared to the other two types of precipitation (stratiform and shallow convection) in both monsoon periods. In conjunction with the remote sensing data (MODIS & TRMM), RSD shows that the presences of cold clouds which extend to deeper altitudes are responsible for the higher D_m during WM season. The immediate significance of the present work is that (1) it contributes to our understanding of seasonal variations of RSD and distribution of different rain types, and (2) it provides information which is useful for quantitative estimation of rainfall from weather radar observations.

© 2016 Elsevier B.V. All rights reserved.

1. Introduction

Knowledge of raindrop size distribution (RSD) and its variability is important for understanding the processes associated with precipitation growth–decay, radio communications, microwave remote sensing, and cloud modeling. The shape of distribution reflects the complex microphysical processes that transform the condensed water into rain. RSD information is one of the fundamentals required for successful modeling of radar meteorology and tropospheric wave propagation. The precipitation forecasting or simulation through numerical weather prediction models relies greatly on raindrop spectra (Curic et al., 2010). The largest source of model uncertainty in the prediction of convective-scale systems is the microphysical parameterization. Several researchers studied the sensitivity of microphysical processes in the model performance (Gilmore et al., 2004b; Cohen and Mc Caul Jr, 2006). Gilmore et al., (2004b) investigated the sensitivity of accumulated precipitation with respect to the particle size distribution. They showed that variations in RSD related to microphysical parameterization within the observed range of uncertainty can cause significant changes in hydrometeor concentration and type. Van den Heever and Cotton (2004) showed that similar variations can change the storm between high-precipitation and low-precipitation types. Ultimately, the extent of modeling is intrinsically dependent on the RSD approximation. Therefore, the physical quantities of raindrops such as size and shape need to be assessed when using NWP models for precipitation forecasting or simulations. For aforesaid applications, accurate measurements of RSD are essential.

Rain attenuation is a major hurdle in the design of radio systems such as terrestrial and satellite communication systems operating at

* Corresponding author at: Department of Physics Coordinator, Semi-arid-zonal Atmospheric Research Centre (SARC) Yogi Vemana University, Kadapa – 516003, Andhra Pradesh, India. Tel.: +91 8562 225455; fax: +91 8562 225419.
E-mail addresses: uvmuralikrishna09@gmail.com (U.V.M. Krishna), krishna.kkreddy@gmail.com (K.K. Reddy), seelabalaji@gmail.com (B.K. Seela), shiro@jamstec.go.jp (R. Shirooka), tliam@pblap.atm.ncu.edu.tw (P.-L. Lin), cjpan@jupiter.ss.ncu.edu.tw (C.-J. Pan).

http://dx.doi.org/10.1016/j.atmosres.2016.01.013
0169-8095/© 2016 Elsevier B.V. All rights reserved.

frequencies above 10 GHz (Chakravarty and Maitra, 2010; Badron et al., 2011). Microwave and millimeter wave attenuation depends considerably on rainrate and raindrop size distribution (Das et al., 2010). Hence, to design radio links for telecommunications and to evaluate the fading caused by rain, it is important to have good RSD models. Several researchers have studied the importance of spatial and temporal characteristics of rainfall such as rainrate and RSD (Berne and Uijlenhoet, 2005). The size of the raindrop is an essential micro-structural property in the modeling and prediction of rain attenuation.

RSD changes in space and time, in correspondence with change in microphysical processes (Rosenfeld and Ulbrich, 2003). Some in-situ measurements of RSD have been conducted using various techniques in various climatic regimes (Tokay and Short, 1996; Testud et al., 2001; Bringi et al., 2003; Schönhuber et al., 2008; Suh et al., 2015). Numerous studies have been carried out to understand the variations of RSD in diurnal, seasonal, intra-seasonal (Reddy and Kozu, 2003; Kozu et al., 2006; Rao et al., 2009; Jayalakshmi and Reddy, 2014), different storms (Maki et al., 2001; Friedrich et al., 2013), and rain types (Tokay and Short, 1996; Reddy et al., 2005; Niu et al., 2010). However, most of these studies have been carried out in the continental regions and are limited over maritime regions. High-temporal RSD characteristics are still sparse in the tropical oceanic region, particularly in the Western Pacific Ocean. There are limited observations over the Pacific Ocean, especially over Palau (7° 20′ N, 134° 28′ E) region (Moteki et al., 2008; Ushiyama et al., 2009; Kozu et al., 2010; Krishna et al., 2014). Variations in the melting layer between westerly and easterly monsoon seasons and their possible mechanisms over Palau islands were illustrated by Krishna et al. (2014). Kozu et al. (2010) studied the gamma RSD model with 1 year data set over Palau islands. Whereas Ushiyama et al. (2009) studied diurnal to interannual variations in RSD characteristics. However, their works are not focused on better rainfall classification and type of precipitation. Hence, in the present study, 4 years of RSD data collected from Joss–Waldvogel disdrometer, lower atmospheric wind profiler and satellite data are utilized to understand RSD variations in two seasons (easterly monsoon—EM and westerly monsoon—WM) as well as three types of precipitation (stratiform, shallow convection, and deep convection).

This paper is structured in the following manner. A short description about the data and methodology used in the present study is presented in Section 2. Observational results are detailed in terms of RSD characteristics of seasonal and type of precipitation in Section 3 followed by possible reasons for the variations in RSD in Section 4. Finally, Section 5 summarizes the conclusion of the present work.

2. Location, data, and methodology

Japan Agency for Marine-Earth Science and Technology (JAMSTEC) is carrying out research at Palau islands (7° 20′ N, 134° 28′ E) called "Pacific Area Long-term Atmospheric observation for Understanding of climate change (PALAU)" project to reveal cloud-precipitation processes and air–sea interactions over the warm-water pool, mainly focusing on seasonal and intra-seasonal variations (Kubota et al., 2005; Moteki et al., 2008; Ushiyama et al., 2009). The Republic of Palau (Fig. 1) is an archipelago of about 350 m high and low islands located in the most western part of the Caroline Islands of the Southwestern Pacific. The Palau islands are almost 800 km equidistant west of the Philippines, north of Irian Jaya, and southeast of Guam. Aimeliik is located in the island of Babeldaob [in the Palau (508 km^2) archipelago], which is one of the largest islands in the Western Pacific Ocean. Field experiments in Palau provided long-term high-temporal resolution observational data over the off-equatorial region of the warm-water pool (Moteki et al., 2008; Ushiyama et al., 2009). For the present study, data collected from the ground-based sensors viz. Joss–Waldvogel disdrometer (JWD), wind profiler radar (WPR), and automatic weather station (AWS) installed by JAMSTEC at Aimeliik observatory (7.3°N, 134.3°E) were used.

Four years (July 2003–June 2007) Joss–Waldvogel disdrometer (Joss and Waldvogel, 1969; Waldvogel, 1974) data are used to measure high-resolution (1-min) RSD at Palau Islands. The JWD is one of the most widely used instruments around the globe for analyzing the RSD and rain characteristics. JWD estimates the diameter of the drops by sensing the voltage induced from the downward displacement of a 50 cm^2 styrofoam cone, once it is hit by raindrops. The output voltage relates to the diameter of the raindrop falling at terminal velocity. It measures hydrometeors with a size ranging from 0.3 to 5.1 mm with an accuracy of 5% and arranges them in 20 channels for 1-min integration time. The raindrop concentration N(D) (mm^{-1} m^{-3}) at an instant of time from JWD is obtained from the following equation:

$$N(D) = \sum_{i=1}^{20} \frac{n_i}{A * \Delta t * v_{(D_i)} * \Delta D_i} \quad (1)$$

where n_i is the number of drops reckoned in the size bin i, A(m^2) and Δt(s) are the sampling area and time, D_i (mm) is the drop diameter for the size bin i, and ΔD_i is the corresponding diameter interval (mm), $v(D_i)$ (m/s) is terminal velocity in the raindrops in the ith channel and is estimated from $v(D_i) = 9.65–10.3\ \exp.(-6^*D_i)$ (Gunn and Kinzer, 1949). From the raindrop concentration $N(D)$, drop diameter (D_i), and terminal velocity $V(D_j)$, radar reflectivity factor Z (mm^6 m^{-3}), and rain rate R (mm/h) are derived by using the equation.

$$Z = \sum_{i=1}^{20} N(D_i) D_i^6 \Delta D_i \quad (2)$$

$$R = 6\pi \times 10^{-4} \sum_{i=1}^{20} V(D_i)\, \mathrm{N}(D_i) D_i^3 \Delta D_i \quad (3)$$

The advantages and drawbacks of this instrument were well documented in the past (Tokay et al., 2001; Tokay et al., 2003; Atlas and Ulbrich, 2006; Tokay et al., 2013). The JWD is unable to resolve the drop size larger than 5–5.5 mm and its calibrations assume that the raindrops are falling at terminal velocity in still air. Under extremely noisy (high rainrates associated with winds) conditions, JWD miscounts drops in lower size bins, particularly for drops of lesser than 1 mm diameter (Tokay et al., 2003). To overcome this problem, an error correction multiplication matrix is provided by the manufacturer based on the correction scheme of Sheppard and Joe (1994). Under intense rainfall events, JWD indicates no drops for the first three to four channels. The multiplicative matrix algorithm does not increase the counts when the channel has no drops (Tokay and Short, 1996). As the dead time correction is not universally utilized within the field (Tokay et al., 2001), we didn't apply correction to the present study. In order to reduce the sampling errors due to insufficient raw drop counts, rainrate less than 0.1 mm/h are discarded in the present study (Tokay and Short, 1996). For the validation of JWD, daily accumulated rainfall amounts measured from JWD were compared with tipping bucket rain gauge of the collocated AWS. AWS provides surface meteorological parameters and also rainfall (rainfall amount and rainrate) data at 1-min sampling interval. Tipping bucket rain gauge measures if only the rainfall accumulation is greater than 0.5 mm. The scatter plot of daily accumulated rainfall amount for 4 years of data sets obtained from JWD and rain gauge is shown in Fig. 1. A linear fit is carried out to the scatter plot. The correlation coefficient is reasonably good between these two measurements. The results suggests that rain integral parameters derived from JWD can be utilized to understand seasonal characteristics of precipitating clouds over Palau region.

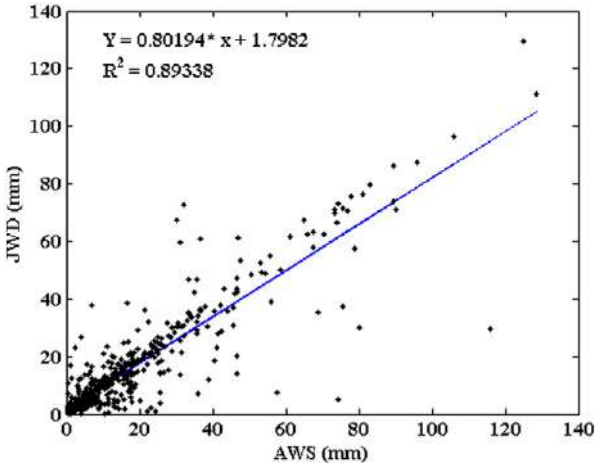

Fig. 1. Scatter plot for daily accumulated rainfall collected from Joss–Waldvogel disdrometer vs tipping bucket rain gauge of the automatic weather station.

The 1-min RSD is fitted with gamma function as suggested by Ulbrich (1983). The functional form of the gamma distribution is given as:

$$N(D) = N_0 D^{\mu} \exp(-\Lambda D) \tag{4}$$

where D(mm) is drop diameter, $N(D)$ is number of drops per unit volume per unit size interval, N_0 ($mm^{-1}\ m^{-3}$) is number concentration parameter, μ is shape parameter, and Λ (mm^{-1}) is slope parameter.

The slope parameter Λ(mm^{-1}) is given by.

$$\Lambda = \frac{(\mu + 4)M_3}{M_4} \tag{5}$$

where μ is the shape parameter without dimensions and is given by

$$\mu = \frac{(11G - 8) + \sqrt{G(G + 8)}}{2(1 - G)} \tag{6}$$

where

$$G = \frac{M_4^3}{M_6 M_3^2} \tag{7}$$

Table 1
Classification of raindrop diameter.

Type of raindrops	Diameter (D) range
Small drops	$D < 1$ mm
Mid-drops	$1 < D < 3$ mm
Large drops	$D > 3$ mm

The normalized intercept parameter N_w ($mm^{-1}\ m^{-3}$) defined by Bringi et al., (2003) as.

$$N_w = \frac{4^4}{\pi \rho_w}\left(\frac{10^3 W}{D_m^4}\right) \tag{8}$$

where ρ_w (1.0×10^3 kg/m^3) represents the density of water and W (kg/m^3) represents the liquid water content for the corresponding size distribution.

The nth order moment of the drop size distribution is expressed as

$$M_n = \int_{D_{min}}^{D_{max}} D^n N(D) dD \tag{9}$$

Here n stands for the nth moment of the size distribution.

The mass-weighted mean diameter D_m, shape parameter μ, and slope parameter Λ are evaluated from the 3rd, 4th, and 6th moments of the size distribution.

$$D_m = \frac{M_4}{M_3} \tag{10}$$

To study the RSD characteristics during different rain types, we have classified the precipitating clouds over Palau into three categories by using WPR moments data. Palau–WPR is a LAP-3000 built by Vaisala Corporation (formerly Radian Corporation) in Boulder, Colorado, with post-processing software from Sonoma Technology Inc. The design is the commercialized version of the systems designed in the NOAA Aeronomy Laboratory (Ecklund et al., 1988; Carter et al., 1995). The operating frequency is 1290 MHz. The WPR has an electronically steered phased array antenna capable of producing five beams. Nominally, the five beam directions are north, south, east, west, and vertical. The off-vertical beams are at an elevation of 74.5 degrees (15.5 degrees down from vertical). The transmitter is capable of producing pulses of four lengths: 400, 700, 1400, and 2800 ns. These correspond to vertical resolutions of 60, 105, 210, and 420 m. The inter-pulse period (pulse repetition frequency) is fully controllable, so the maximum range is limited

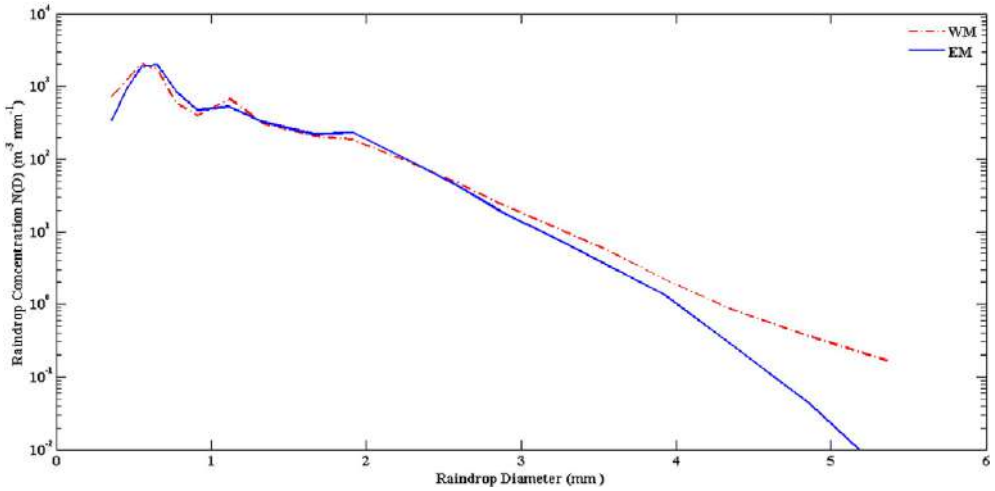

Fig. 2. Mean raindrop concentration during easterly monsoon and westerly monsoon precipitation.

Table 2
Mean, maximum, and standard deviation of $N(D)$ for each drop diameter class during EM and WM seasons.

Sl. no.	Drop diameter	Mean $N(D)$		Maximum		Standard deviation	
		EM	WM	EM	WM	EM	WM
1	0.359	340.74	730.70	24,541.74	112,495.5	282.78	842.75
2	0.455	920.03	1205.21	67,919.8	81,225.07	641.25	787.74
3	0.551	1863.19	2050.29	180,064.2	128,520.2	1893.38	2161.61
4	0.61	1973.58	1708.10	57,198.21	56,012	2678.55	2517.64
5	0.771	866.56	595.42	23,118.79	20,325.66	945.48	522.95
6	0.913	467.70	399.70	5849.93	5427.61	111.75	103.86
7	1.116	522.35	677.61	6389.12	103,234.8	208.69	852.92
8	1.331	327.61	310.53	1581.42	1791.82	197.46	195.89
9	1.506	261.08	254.85	1217.28	1715.44	214.90	208.96
10	1.665	221.01	206.90	2052.05	984.43	218.96	199.12
11	1.912	229.75	187.26	2024.74	1355.70	280.77	202.87
12	2.259	100.49	96.64	557.89	638.89	155.57	136.12
13	2.584	43.87	47.57	245.58	335.16	72.68	75.02
14	2.869	19.15	24.08	194.55	194.55	32.94	40.84
15	3.198	8.77	12.12	124.12	134.91	16.12	22.17
16	3.544	3.58	5.68	68.39	103.81	7.05	11.02
17	3.916	1.39	2.25	36.89	48.31	2.92	4.52
18	4.35	0.28	0.87	14.17	22.51	0.59	1.88
19	4.859	0.04	0.36	7.06	19.26	0.08	0.85
20	5.373	0.004	0.16	31.27	254.97	0.009	0.3

only by the strength of the returned signals (depends on the background meteorological conditions). Sampling of the returned signal (i.e. the range gates) can be done at intervals that are multiples of the pulse lengths. This radar operates continuously in pulse mode, using three beams [one vertical and two oblique (north and east)]. It is configured to operate in two modes (hereafter called "low/boundary layer mode" and "high/precipitation mode"), which correspond to two different vertical resolutions (respectively, 58 and 202 m) and two different vertical ranges (respectively, from 130 to 4120 m and from 332 to 11,260 m). The two modes are interlaced in time. A dwell time of 35 s is used to get the data from each pointing beam. For each cycle of (low- and high-mode) observations about three-and-a-half-minute time is required. The in-house digital signal processor of the LAP-3000 system can calculate moments and winds apart from spectra and also store data in the radar computer. In the present study, WPR is used only for classifying the precipitation into three categories, namely, stratiform (ST), deep convection (DCT), and shallow convection (SCT) by examining the vertical structure of radar reflectivity and Doppler velocity based on the original algorithm proposed by Williams et al., (1995).

In addition to the ground-based sensors, we have utilized precipitation radar (PR) onboard Tropical Rainfall Measuring Mission (TRMM) satellite data for estimation of storm top height. The measurement of TRMM provides different parameters including rain intensity, rain type, height of the melting layer, and the storm top height as a function of range at its operational frequency 13.8 GHz in 0.5° × 0.5° grid. PR has a vertical resolution of 250 m and horizontal resolution of 4.3 km. It covers the tropical region from 37°S to 37°N. The data description and algorithm for level 3 A25 data were given in TRMM-PR algorithm instruction manual for version 7. For details, please refer to Iguchi et al. (2000) and Kummerow et al. (2001). Apart from this, the cloud effective radius (CER) values for ice, water, and mixed state particles from Moderate Resolution Imaging Spectroradiometer (MODIS) level 3 were also utilized. MODIS level 3 daily global atmospheric data product (MOD08_D3) consists of 1° × 1° grid average values of atmospheric parameters related to aerosol particle properties, water vapor, cloud optical and physical properties (Remer et al., 2005). Multispectral reflectance is used to retrieve CER for liquid and ice phases. The basic physical principle behind the retrieval of CER is the bispectral solar reflectance method first described by Nakajima and King (1990) and applied to airborne data. An overview of the MODIS cloud product algorithms along with example results is provided in Platnick et al. (2003) and King et al. (2003). For the present study, 4 years (July 2003–June 2007) of TRMM and MODIS data were utilized.

3. Results

To study the seasonal variation in RSD characteristics, the precipitation datasets are classified into WM and EM seasons as defined by Kubota et al. (2005). Westerly winds prevailed from June to November over Palau region. The onset of WM season can be defined as the first day that the 5-day running mean zonal wind exceeded 5 ms^{-1}. Onset of westerly monsoon occurred during May and withdrawal occurred during November in the year 2003. However, onset of westerly monsoon occurred in June for 2004, 2005, and 2006 and withdrawal occurred during November for 2004 and October for 2005 and 2006. JWD and WPR measurements are available for four WM (2003, 2004, 2005, and 2006) and four EM (2004, 2005, 2006, and 2007) seasons. We have analyzed 4 years of data to understand the RSD characteristics during two monsoon seasons and three rain types.

3.1. Seasonal variation of RSD

The variation in the mean raindrop concentration, $N(D)$, with raindrop diameter D in WM and EM season for 4 years of data is depicted in Fig. 2. $N(D)$ is represented in logarithmic units to accommodate its large variations. In this paper, the raindrops below 1 mm diameter and above 3 mm diameter are considered as small and large drops, respectively. Raindrops from 1 to 3 mm diameter are considered as midsize drops (Tokay et al., 2008; Rao et al., 2009). These raindrop diameter classes are given in Table 1. From the figure, it is apparent that the number concentrations of mid and large drops are higher in WM season when compared to EM season, whereas the small drops have same number concentration in both the seasons. However, the midsize drops up to ~2.6 mm diameter have small concentration in WM than EM season. The mean along with standard deviation of $N(D)$ for different drop diameter classes is given in Table 2. To ascertain the differences in $N(D)$, a statistical test is applied to the drop concentrations of two seasons. The Student t test results disproves the null hypothesis H0 ($N(D)$ during WM season = N(D) during EM season) for all diameter classes except for the diameter size 2.584 mm. This

Table 3
Statistical measure of disdrometer-derived rainrates (classified into 9 rainrate classes) for EM and WM seasonal raindrop size distribution sets.

Class	Rainrate threshold	Easterly monsoon			Westerly monsoon		
		No. of data	Mean (mm/h)	Standard deviation	No. of data	Mean (mm/h)	Standard deviation
1	1 ≤ RR < 2	6408	1.430	0.287	10,930	1.430	0.286
2	2 ≤ RR < 4	6228	2.869	0.573	9469	2.849	0.573
3	4 ≤ RR < 6	3400	4.911	0.579	4486	4.910	0.576
4	6 ≤ RR < 8	1961	6.911	0.575	2544	6.925	0.569
5	8 ≤ RR < 10	1355	8.937	0.577	1563	8.920	0.577
6	10 ≤ RR < 30	4886	17.491	5.567	6155	17.805	5.754
7	30 ≤ RR < 60	1772	40.472	8.056	2201	40.016	8.265
8	60 ≤ RR < 90	232	69.059	7.585	458	72.028	8.043
9	RR ≥ 90	76	94.851	4.467	107	108.431	31.966

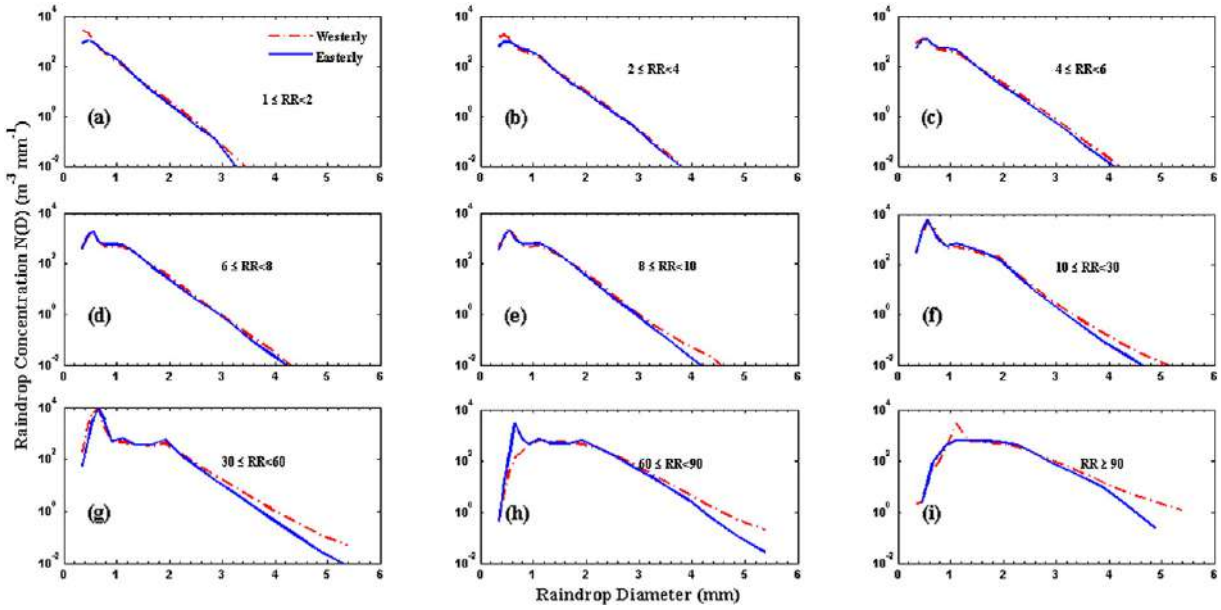

Fig. 3. Mean RSD during easterly monsoon and westerly monsoon precipitation for different rainrates.

indicates that the N(D) distributions are different during WM and EM seasons. These results are consistent with the observations of Tokay et al. (2002). They observed more number of large (small) drops in EM (WM) season over Amazon basin in the Southern Hemisphere. However, Palau is situated in the Northern Hemisphere. Ushiyama et al. (2009) found increasing (decreasing) values of mean drop diameters during El Nino (La Nina) years of westerly monsoon period over Palau region. More number of small drops in north-east monsoon and large number of big drops in south-west monsoon are observed by other researchers over southern India (Reddy and Kozu, 2003; Kozu et al., 2006; Rao et al., 2009; Jayalakshmi and Reddy, 2014). Chakravarty and Raj (2013) observed more number of large drops in post monsoon and medium and small drop in monsoon season over tropical western India. However, over eastern India, higher concentration of large (small) drops in pre-monsoon (monsoon) months was reported by Chakravarty et al. (2013). Intraseasonal variation of RSD in response to Madden–Julian Oscillation (MJO) was studied by Kozu et al. (2005) over Indonesia. They found broader (narrow) RSD during non-active (active) phases of MJO. Recently, Marzuki et al., (2015) reported higher concentration of medium and large-size drops in inactive phase of MJO than active phase for the same Indonesia region.

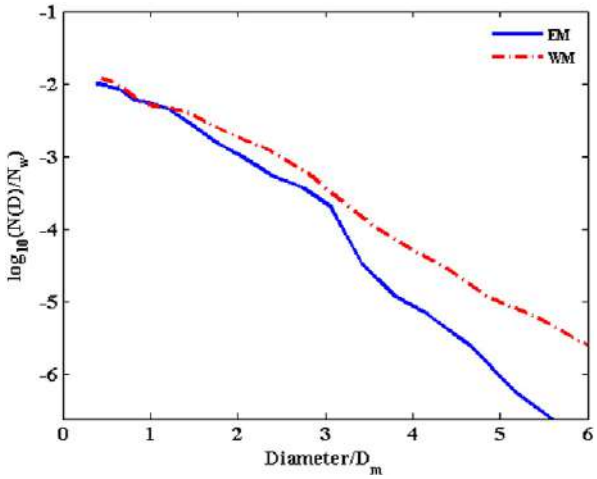

Fig. 4. Normalized gamma RSD for easterly monsoon and westerly monsoon precipitation.

Four years of data collected from JWD are stratified into nine rainrate (RR) classes ($1 < RR < 2$, $2 < RR < 4$, $4 < RR < 6$, $6 < RR < 8$, $8 < RR < 10$, $10 < RR < 30$, $30 < RR < 60$, $60 < RR < 90$ and $RR > 90$). Nine rainrate classes are selected based on these two criteria: (1) the number of data (number of one minute data samples) points should be large in each class, so that the results will be strong, and (2) the mean RR for each class should be nearly equal in both the seasons. Rainrate statistics of the EM and WM rainfall for different rainrate classes are shown in Table 3. From the table, it is clear that mean value of each rainrate class is approximately equal in both the seasons except for last two rainrate classes and each rainrate class has higher duration in WM than EM seasons. The mean of raindrop concentration, $N(D)$ variations with raindrop diameter D for nine rainrate classes in EM and WM seasons are given in Fig. 3. The distribution is nearly linear at low rainrates (<8 mm/h) and show curvature at larger rainrates (>8 mm/h). It is apparent from the figure that the RSD concentrations of small drops are either equal or very slightly higher in EM than WM in all the rainrate classes except for the first two rainrate classes (<4 mm/h). However, for the rainrate classes above 8 mm/h, concentration of larger drops in WM season is higher than EM season. The difference in RSD concentration of larger drops during WM and EM season increases with the increase in rainrate class. In both the seasons, concentration of small drops decreases and large drops increases with increase in rainrate. Similar type of phenomena was observed by Kozu et al. (2006) for oceanic regions (Singapore and Indonesia) as well as for continental region (Gadanki). The significant difference in $N(D)$ from WM to EM season is pronounced in the rainrate classes above 8 mm/h. Lower rainrate classes (<8 mm/h) show unimodal distribution and higher rainrate classes (>8 mm/h) show bimodal distribution. The possible reasons for these distribution variations are given in Section 3.2. A difference in RSD of EM and WM can be seen from Figs. 2 and 3, and these distributions are represented without normalization. In order to ascertain the difference in RSD in two seasons, Testud et al. (2001) method is applied. The averaged normalized distribution of RSD for both the seasons is depicted in Fig. 4. From this figure, it is observed that clear demarcation between EM and WM which imply that the shapes of RSD are different in both the seasons.

The important application of RSD is its utilization in cloud modeling studies. To facilitate this, WM and EM precipitation RSDs are fitted to gamma distribution (Eq. 4). The shape parameter (μ) describes the breadth of RSD and determines whether the RSD is of concave

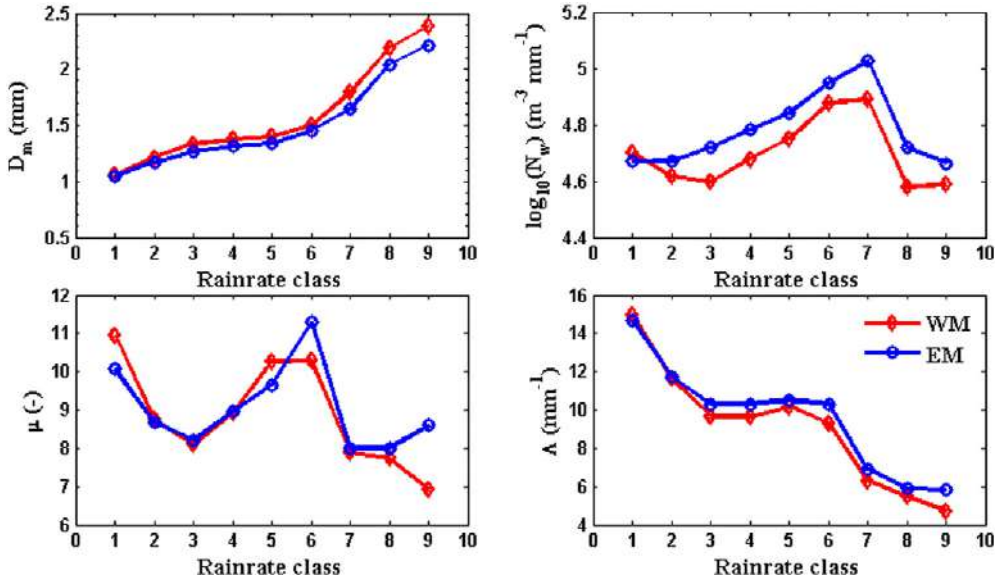

Fig. 5. Variations in mean values of D_m, $\log_{10}(N_w)$, μ, and Λ in each rainrate class during easterly monsoon and westerly monsoon precipitation.

downward (μ > 0), upward (μ < 0), or of exponential (μ = 0) shape (Ulbrich, 1983). The slope parameter (Λ) characterizes truncation of RSD tail along D, for example, small (large) Λ indicates an extension of the RSD tail to larger (smaller) D. The normalized intercept parameter N_w represents $N(D)$ when D approaches to its minimum value. The variation of mass-weighted mean diameter D_m, normalized intercept parameter N_w, shape μ and slope parameter Λ as a function of rainrate class for WM and EM seasons is shown in Fig. 5. It can be noticed from this figure that the mean values of D_m show a similar pattern of variation, i.e., a continuous increase with rainrate in both the seasons. This is due to decrease of small drops and increase of large drops with increase in rainrate. This feature is consistent with the observations of other researchers (Testud et al., 2001; Rosenfeld and Ulbrich, 2003; Rao et al., 2009; Jayalakshmi and Reddy, 2014). The mean D_m values of WM season are higher compared to EM seasons in all the rainrate classes. The lower D_m values in all the rainrate classes of EM are due to relatively large number of small drops compared to WM seasons in all the rainrate classes. The mean D_m value varies between 1.05 and 2.4 mm in WM and it ranges from 1.04 to 2.2 mm in EM season. The difference in mean D_m between WM and EM season increases with rainrate class and it varied from 0.012 to 0.175 mm. Jayalakshmi and Reddy (2014) reported higher values for the difference in mean D_m (varies from 0.15 to 0.32 mm) between south-west and north-east monsoon seasons over continental location. The mean normalized intercept parameter $\log_{10}N_w$ increases up to rainrate class 7 (below 60 mm/h) and then decreases in both seasons. The mean value of $\log_{10}N_w$ varies between 4.57 and 4.89 during WM and is between 4.66 and 5.03 during EM season.

Table 4
Mean values of D_m, $\log_{10}(N_w)$, μ, and Λ during easterly monsoon and westerly monsoon precipitation.

Rainrate class	Easterly monsoon				Westerly monsoon			
	D_m	$\log_{10}(N_w)$	μ	Λ	D_m	$\log_{10}(N_w)$	μ	Λ
1	1.04	4.67	10.06	14.69	1.05	4.69	10.94	14.96
2	1.17	4.67	8.65	11.75	1.20	4.61	8.73	11.62
3	1.26	4.72	8.21	10.29	1.33	4.59	8.09	9.66
4	1.31	4.78	8.95	10.3	1.37	4.67	8.92	9.64
5	1.34	4.84	9.66	10.5	1.39	4.74	10.27	10.17
6	1.45	4.94	11.28	10.3	1.49	4.87	10.28	9.28
7	1.64	5.02	8.01	6.87	1.78	4.88	7.87	6.28
8	2.04	4.71	8.0	5.89	2.18	4.57	7.73	5.45
9	2.21	4.66	8.6	5.82	2.38	4.58	6.92	4.71

The mean value of $\log_{10}N_w$ is higher in EM than WM in all the rainrate classes except at RR < 2 mm/h. The mean value of Λ in both monsoons shows a monotonous decrease with increase in rainrate. The mean Λ values are found to be in the range of 4.71–14.96 mm^{-1} (5.8–14.69 mm^{-1}) in WM (EM) season. Presence of relatively large drops in WM season decreases the mean Λ. This feature is more predominant at higher rainrates. Hence the seasonal difference is also significant at these rainrates. On the other hand, the seasonal variation in μ is not clear. The variation of μ with rainrate is small in comparison with the variation of Λ. The mean value of μ is higher in WM precipitation for rainrate classes 1 < RR < 2, 2 < RR < 4 and 8 < RR < 10 mm/h and is lower for the remaining classes than EM precipitation. The μ values for WM (EM) season are in the range of 10.94–8.1 (10.07–8.21) up to a rainrate of 4 mm/h (a decreasing trend with increasing rainrate), increases to 10.28 (11.28) at 30 mm/h, and then decreases again to 6.92 (8.0) for rainrate >30 mm/h. Mean values of D_m, N_w, μ, and Λ for WM and EM seasons at different rainrate classes are given in Table 4.

A better way to represent RSD characteristics is possible by considering the mean value of the RSD parameters (Bringi et al., 2003; Marzuki, et al., 2010). Fig. 6 shows the variation of mean values of $\log_{10}N_w$ (along with standard deviation) with D_m for different rainrate classes in both the seasons. It is evident from this figure that the mean value of D_m increases with rainrate. The mean values of $\log_{10}N_w$ show a wide and large range for higher values of D_m, whereas this range tends to decrease for lower D_m values. The mean values of D_m ($\log_{10}N_w$) are larger (smller) in WM season than EM season in all the rainrate classes except at class 1. It indicates that the WM season RSD is somewhat broader (more larger drops and smaller drop concentration) than those in EM season. Further, the difference in mean values of $\log_{10}N_w$ between WM and EM seasons increases with the increase in rainrate class. However, the standard deviation (within a rainrate class) decreases with the increase in raindrop diameter in both the seasons.

3.2. RSD variation in stratiform, deep, and shallow convective precipitation

RSD structures are significantly different during convective regimes than that of stratiform regimes. For instance, Ulbrich and Atlas (2007) argued to use different Z–R relations in different rain types by showing changes in RSD parameters during stratiform to convective precipitation. Variations in RSDs during stratiform and convective rain type using two different disdrometers in different climatic regimes were studied by Bringi et al. (2003). Tokay and Short (1996) demonstrated

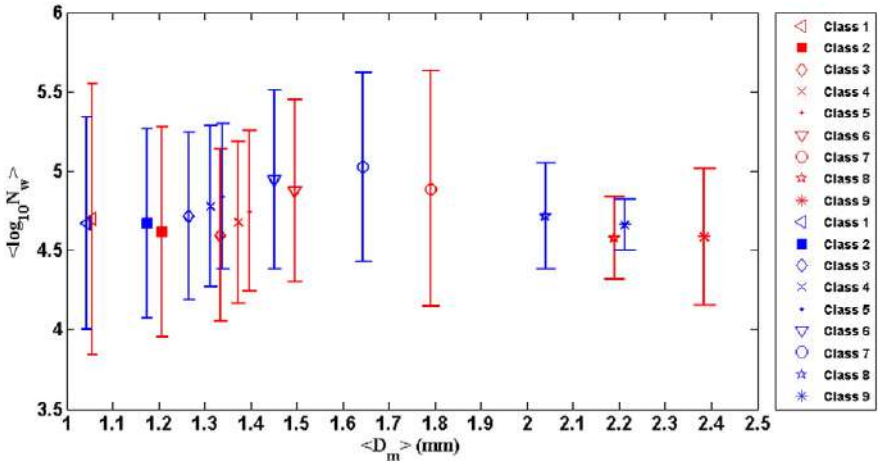

Fig. 6. Variation of mean normalized intercept parameter ($\log_{10}N_W$) (along with ±1 standard deviation) with mass-weighted mean diameter (D_m) for EM (blue color) and WM (red color) precipitation in different rain classes.

that raindrop parameters are sequentially altered from convective precipitation to stratiform precipitation in a tropical system. It is well known that the microphysical dynamics of raindrop spectra is different in different rain types. Due to this reason, we have investigated raindrop spectra characteristics of three precipitation types (stratiform, deep convection, and shallow convection). Identification of RSD features with these three precipitation types is useful and important for numerous applications (Kozu et al., 2006). There are a number of rain classification schemes proposed by many researchers using different ground-based instruments like disdrometer, profiler, and radar (Steiner et al., 1995; Tokay and Short, 1996; Rao et al., 2001; Bringi et al., 2003; Thurai et al., 2015).

Vertical profiles of radar reflectivity and Doppler velocity collected from WPR are used to classify precipitation into three types on the basis of three criteria. *1*). If there is a clear signature of bright band (the region just below zero degree isotherm having enhanced reflectivity which is produced by liquid coated ice particles) observed by WPR then the corresponding rainfall at the ground is considered as stratiform. *2*). If there is an enhanced turbulence above the zero-degree isotherms with the absence of bright band then the corresponding rain at ground is considered as deep convection. *3*). Rainfall at the ground level is considered as shallow convection if the clouds are not extended beyond zero degree isotherm level with turbulence within the cloud system (Williams et al., 1995). The only difference between the present rainfall classification and Williams et al. (1995) classification is that they classified rain into stratiform, mixed, shallow, and deep convection, but in the present study, we have classified them into three types only (stratiform, shallow, and deep convection). As an example for the classifications of three precipitations on the basis of the above three criteria, vertical profile of radar reflectivity on 7th July 2003 is shown in Fig. 7. Fig. 8 (a andb) shows RSD characteristics of stratiform, deep, and shallow convective precipitation observed during WM and EM seasons. A clear difference in raindrop concentration between convective (deep and shallow) and stratiform precipitations can be seen in both the seasons. The mean concentration of raindrops (small, midsize, and large) is higher for deep convective precipitation and smaller for stratiform precipitation during both monsoon seasons. Similar type of distribution was observed by other researchers for continental locations (Niu et al., 2010; Chen et al., 2013; Jayalakshmi and Reddy, 2014). Mean raindrop concentration is intermediate for shallow convective precipitation. In both seasons, only small and mid-drops are observed in stratiform precipitation. Because of higher extent of clouds in deep convection, there is sufficient time for collision and coalescence process leading to the growth of raindrops as compared to the other two types of precipitations (shallow convection and stratiform). In order to understand the seasonal variation in RSD in different rain types, we have plotted the concentration of raindrops against drop diameter for different rain types in Fig. 8 (c–e). In all types of precipitation, concentration of smaller drops in EM season is the same (or slightly higher) as that in WM season. Whereas the concentration of larger drops is higher in WM compared to EM season. Raindrops with diameter below ~1.4 mm have higher concentration in EM season for stratiform precipitation. However, the concentration of raindrops is same during both monsoon periods in stratiform precipitation for a diameter greater than 1.4 mm. The raindrop concentration above 2 mm diameter is higher in WM season than in EM season for both deep and shallow convective precipitation. The deep convective precipitations of both the seasons show a bimodal distribution (Steiner and Waldvogel, 1987), whereas stratiform and shallow convection show unimodal distribution. The bimodal distribution (multiple peaks) in the deep convection may be due to the melting/breakup process at the freezing level and coalescent growth of cloud droplet (Gossard et al., 1990) or occurrence of secondary ice generation and super-cooled drizzle near the melting level (Zawadzki et al., 2001).

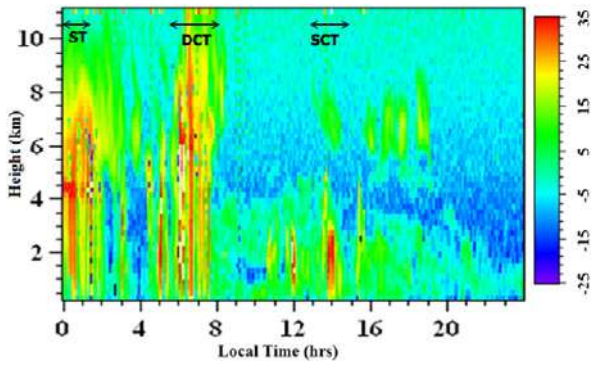

Fig. 7. Vertical profile of signal-to-noise ratio (on 07 July 2003) showing the three types of precipitation. Here ST represents stratiform precipitation, DCT represents deep convective precipitation, and SCT represents shallow convective precipitation.

The variation of mean values of intercept parameter, $\log_{10}N_w$ (shown as $<\log_{10}N_w>$) with the mean values of mass-weighted mean diameter, D_m (shown as $<D_m>$) for different raintypes in EM and WM seasons are shown in Fig. 9. The standard deviation of the intercept parameter is also shown in the figure. This figure evidently indicates an inverse relationship between $<D_m>$ and $<\log_{10}N_w>$. For example, during deep convective precipitation, $<D_m>$ is found to be 1.48 mm with $<\log_{10}N_w> = 4.67$ in WM period. On the other hand, relatively lower $<D_m> = 1.44$ mm and higher $<\log_{10}N_w> = 4.8$ are observed in EM period. During shallow convection of WM (EM) season $<D_m> = 1.14$

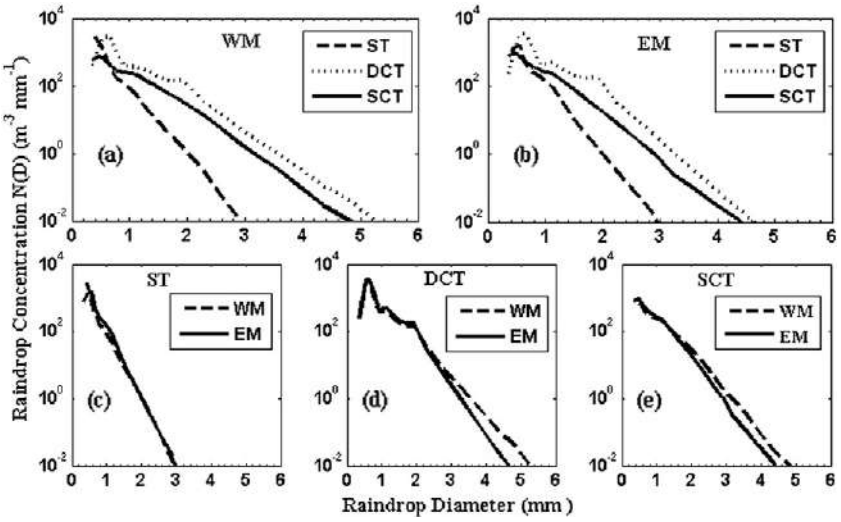

Fig. 8. Variation of RSD with rain type during easterly monsoon and westerly monsoon precipitation.

(1.00) mm and $<\log_{10}N_w> = 4.5$ (4.8) are observed. Bringi et al. (2003) studied the variation of $<D_m>$ and $<N_w>$ for a wide range of locations from near equator to subtropics to oceanic (referred as maritime-like) and high plains to continental to subtropics to tropics (referred as continental-like) for convective precipitation. They found maritime-like clusters are located around $<D_m>$ ~ 1.5–1.75 mm and $<N_w>$ ~ 4–4.5 while continental-like cluster is characterized by $<D_m>$ ~ 2–2.75 mm and $<N_w>$ ~ 3–3.5. Our results are different from their observations and are somewhat closer to the maritime-like cluster in both EM and WM seasons. However $<D_m> = 0.79$ mm (0.9 mm) and $<\log_{10}N_w> =$ 5.02 (4.69) are observed in stratiform precipitation during WM (EM) period. These results are consistent with the results of Testud et al. (2001) and Marzuki et al. (2013). Further, the values of mean D_m ($\log_{10}N_w$) are larger (smaller) during WM period than in EM period for deep and shallow convective precipitation. However, in stratiform precipitation, D_m is lower in WM than in EM season and this may be due to higher percentage of stratiform precipitation with lower bright band height in WM than EM season (Krishna et al., 2014).

Distribution of D_m for stratiform, deep convective, and shallow convective precipitation during EM and WM periods are represented with box and whisker plot in Fig. 10. In this plot, the boxes represent data between the first and third quartiles and the whiskers show data from 12.5 to 87.5 percentiles. In the figure, the symbol "×" represents 99% and 1% significant levels and the horizontal line with in the box represents the median value of D_m. The median value of D_m is higher for deep convective precipitation, smaller for stratiform precipitation, and intermediate for shallow convective precipitation in both EM and WM period. Median value of *Dm* is the same in both WM and EM monsoon periods for deep convective precipitation, whereas the median value of D_m is higher in WM period as compared to EM period for shallow convection precipitation. A reverse trend with higher D_m is observed in EM as compared to WM season for stratiform precipitation. The mean values along with their standard deviation of D_m values for the three types of precipitations are given in Table 5.

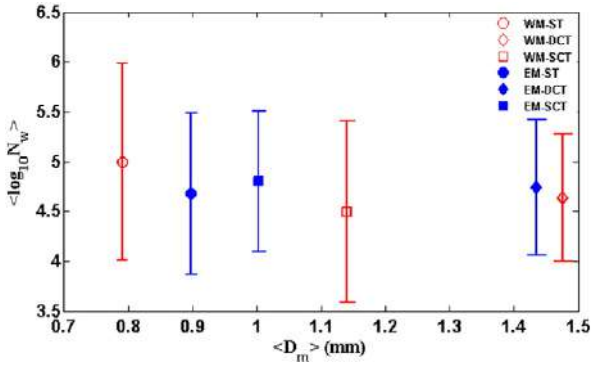

Fig. 9. Mean and standard deviation of normalized intercept parameter ($\log_{10}N_w$) versus average mass-weighted mean diameter (D_m) for stratiform, deep convective, and shallow convective precipitation during easterly monsoon and westerly monsoon precipitation.

3.3. Implications of seasonal differences in RSD

The major uncertainty in radar rainfall estimation is due to the variability of RSD. These variations affect the Z–R relation, where Z represents radar reflectivity and R represents rainrate (Chapon et al., 2008). RSD varies from one climatic region to the other, from one storm to the next and even within a storm. A number of studies offered a single, dual, or multiple Z–R relations (Tokay and Short, 1996; Atlas et al., 1999; Marzuki et al., 2013). The leading cause for these observed differences is due to the difference in type of precipitation (i.e. convective and stratiform precipitation). Numerous researchers have shown that the RSD structures are significantly different during convective regimes than that of stratiform regimes. For instance, Ulbrich and Atlas (2007) argued to use different Z–R relations in different rain types by showing changes in RSD parameters during stratiform to convective precipitation.

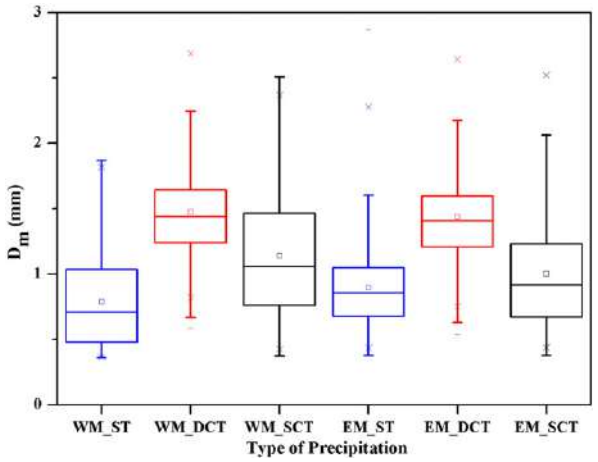

Fig. 10. Box and whisker plot of $<D_m>$ during stratiform, deep convective, and shallow convective precipitation.

Table 5
Mean and standard deviation of D_m for three types of precipitations during easterly monsoon and westerly monsoon precipitation.

Type of precipitation	Mass-weighted mean diameter (D_m)							
	Easterly monsoon				Westerly monsoon			
	Min	Max	Mean	SD	Min	Max	Mean	SD
Stratiform	0.414	2.472	1.206	0.298	0.368	5.300	1.192	0.326
Deep convection	0.374	5.303	1.042	0.435	0.359	5.300	0.905	0.476
Shallow convection	0.376	3.004	1.002	0.428	0.373	3.938	1.140	0.470

Differences in RSD during different rain type, season, and location have implications on Z–R relations. Normally, weather radars estimate rainfall using the relationship between radar reflectivity factor (Z) and rainfall intensity (R), i.e., $Z = A^*R^b$. The coefficient "A" infers presence of smaller or bigger raindrops while the exponent "b" infers microphysical processes. Large exponent value ($b > 1$) characterizes size or mixed controlled case while linear Z–R relationship ($b \sim 1$) is associated with number controlled case for steady and statistically homogeneous or equilibrium rainfall (Atlas et al., 1999; Atlas and Williams, 2003; Steiner et al., 2004; Sharma et al., 2009). Adapting the Z–R relationship to different rain types within a given storm is seen as a promising way to improve radar quantitative precipitation estimation (Waldvogel, 1974). We have analyzed Z–R relations using the linear regression on log-transformed values of R and Z. Table 6 details Z–R relations during different seasons and rain types. We can notice an appreciable variability in the coefficients of Z–R relation. During WM season, the coefficient "A" and the exponent "b" show higher values than EM season. These higher values are consistent with larger D_m values associated with WM season. The coefficient and the exponent values for stratiform, deep convective, and shallow convective precipitation agree well with the previous results of Kozu et al. (2006) and Marzuki et al., (2013). Hence, different RSDs at different location, season, and rain type leads to different Z–R relationships. Thus, the usage of a single Z–R relationship may underestimate rainfall at one site and overestimate at other site.

4. Discussion

The differences in microphysical processes from EM to WM seasons play a crucial role in modifying RSD. RSD evolves into an equilibrium distribution under the influence of processes such as collision, coalescence, and breakup, if the 0 °C isotherm level is sufficiently high (Hu and Srivastava, 1995; Atlas and Ulbrich, 2006). Therefore, if the height of melting level is different in these seasons, it may cause some differences in RSD at the surface. Krishna et al. (2014) found a significant difference in the height of the melting level from EM to WM seasons over Palau. They found that the mean bright band height is ~4.8 km during EM season, whereas it is ~4.6 km during WM season. In addition, the convective activity is different in these seasons. The percentage of occurrence of convective activity is larger in WM season than in EM season (Fig. 11). This indicates that the storms in WM season are deeper as compared to storms in EM season. These deep and intense convective activities have stronger updrafts which affect the rain RSD in two ways: drop sorting and enhancing the collision–coalescence process. Strong updrafts carry small drops aloft into divergent regions but allow bigger drops to precipitate locally, thereby increasing D_m values.

Table 6
Radar reflectivity and rainrate (Z–R) relations for EM and WM and their rain types.

Monsoon	Seasonal		Stratiform		Deep convection		Shallow convection	
	A	b	A	b	A	b	A	b
Westerly	165.66	1.45	291.58	1.37	133.14	1.49	198.77	1.29
Easterly	184.79	1.33	280.91	1.38	165.77	1.33	150.62	1.38

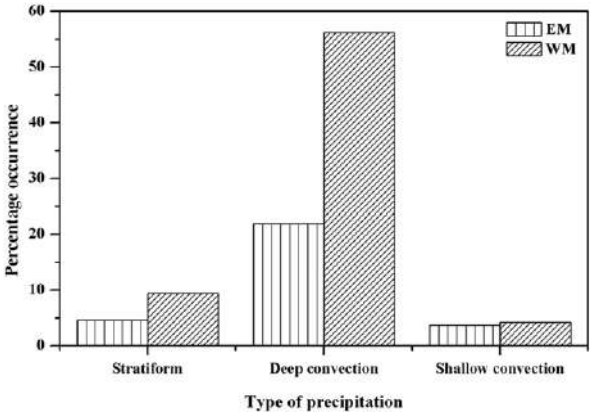

Fig. 11. Percentage occurrence of stratiform, deep convective, and shallow convective precipitation during EM and WM seasons.

The updrafts can also hold drops aloft, thereby increasing the chance of collision and also changing the size of the drop. Therefore, one can expect large D_m values during WM season.

Further, the storm top height is an important parameter in stratiform clouds. In deep stratiform clouds, the ice crystals have sufficient time to grow by vapor deposition and aggregation to large snowflakes, which in turn produces relatively large drops while crossing the melting level. Box and whisker plot of storm top height measured using TRMM-PR during EM and WM seasons for the period 2003–2007 is shown in Fig. 12. The median value of storm top height is higher in WM period as compared to EM period. The percentage occurrence of storm top height greater than 4.6 km is higher (40%) in WM season than in EM season (17.2%). Hence, cold rain is dominant in WM season. On the other hand, percentage occurrence of warm rain is higher during EM season than in WM season (14.2% and 10% of storm top height <4.6 km during EM and WM season, respectively). These results are strongly supported by higher values of mean cloud effective radii of ice phase particle and smaller values of water phase in WM season than EM season (Fig. 13). Therefore, the storm top heights are consistent with the observed RSD variations during EM and WM seasons. From the microphysical perspective, stratiform rain results via the melting of snowflakes and/or tiny graupel or rimed particles. If the bright band is "strong," then it reflects melting of large, low-density dry snowflakes into rain, whereas if the bright band is "weak," then it may reflect the melting of tiny, compact graupel or rimed snow particles (Fabry and Zawadzki, 1995). In fact, the transition from large, dry snowflakes to tiny, compact graupel, or rimed particles during a stratiform rain

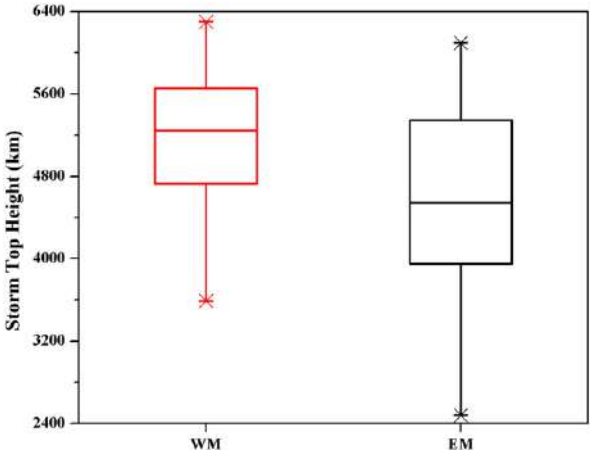

Fig. 12. Box and whisker plot of mean storm top heights during easterly monsoon and westerly monsoon precipitation for the period 2003 to 2007.

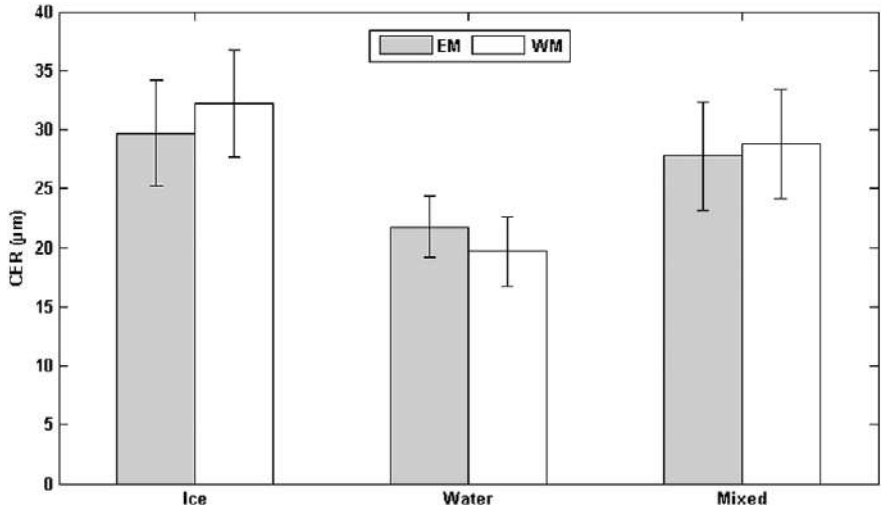

Fig. 13. Mean values of cloud effective radius for different phases of hydrometeors during easterly monsoon and westerly monsoon precipitation of 2003–2007.

event leads to the so-called N_0-jump effect (Waldvogel, 1974). In essence, the larger, low-density snowflakes lead to RSD that has smaller $<\log_{10}N_w>$ and larger $<D_m>$ relative to tiny, compact graupel or rimed snow particles.

5. Conclusions

Four years of RSD measurements made with Joss–Waldvogel disdrometer, wind profiler radar, along with ancillary information from TRMM and MODIS satellite data were analyzed to understand WM and EM seasonal behavior. The observational results revealed that the number concentration is greater in WM season compared to EM season for larger drops. Smaller raindrops have the same number concentration in both the seasons. The RSD stratified on the basis of rainrate showed that the concentration of small drops are almost the same in both EM and WM season for the rainrate classes below 8 mm/h and the concentration of larger drops is slightly higher in WM season than EM season for the same rainrate classes. However, for the rainrate classes above 8 mm/h, concentration of larger drops in WM season is higher than EM season. The higher percentage of convective activity in WM season and the difference in microphysical phenomenon are responsible for the variations in RSD during these seasons. The RSD fitted to gamma function showed that the mean value of D_m is higher in WM in all the rainrate classes. Furthermore, the difference in mean D_m between WM and EM season increases with rainrate. The mean value of $\log_{10}N_w$ is higher in EM than WM in all the rainrate classes except at RR < 2 mm/h. However, the seasonal variations in slope and shape parameters are not as much as observed in D_m and N_w. The RSD shows significant variations in different rain types (stratiform, deep convection, and shallow convection). The concentration of smaller drops is slightly higher for these three types of precipitation during EM season whereas the concentration of midsize and larger drops is higher for deep and shallow convection in WM season. The mean value of D_m ($\log_{10}N_w$) is higher (lower) in deep convective precipitation compared to other types of precipitation in both the monsoon seasons. The transition of large, dry snow flakes to tiny, compact graupel, or rimed particles results in larger D_m and smaller N_w during deep convective precipitation. Different RSDs during different seasons and rain types show different Z–R relationships.

Acknowledgments

We acknowledge the Japan Aerospace Exploration Agency (JAXA), Tropical Rainfall Measuring Mission (TRMM), and MODIS for providing the data. The authors are thankful to the two anonymous reviewers and the editor for their valuable suggestions and comments for the better improvement of the manuscript.

References

Atlas, D., Ulbrich, C.W., 2006. Drop size spectra and integral remote sensing parameters in the transition from convective to stratiform rain. Geophys. Res. Lett. 33 (16), L16803.
Atlas, D., Williams, C.R., 2003. The anatomy of a continental tropical convective storm. J. Atmos. Sci. 60, 3–15.
Atlas, D., Ulbrich, C.W., Marks Jr., F.D., Amitai, E., Williams, C.R., 1999. Systematic variation of drop size and radar-rainfall relations. J. Geophys. Res.-Atmos. 104, 6155–6169.
Badron, K., Ismail, A.F., Din, J., Tharek, A.R., 2011. Rain induced attenuation studies for V-band satellite communication in tropical region. J. Atmos. Sol. Terr. Phys. 73, 601–610.
Berne, A., Uijlenhoet, R., 2005. A stochastic model of range profiles of raindrop size distributions: application to radar attenuation correction. Geophys. Res. Lett. 32, L10803 10.1029/2004GL021899.
Bringi, V.N., Chandrasekar, V., Hubbert, J., Gorgucci, E., Randeu, W.L., Schoenhuber, M., 2003. Raindrop size distribution in different climatic regimes from disdrometer and dual-polarized radar analysis. J. Atmos. Sci. 60, 354–365.
Carter, D., Gage, K.S., Ecklund, W.L., Angevine, W.M., Johnston, P.E., Riddle, A.C., Wilson, J., Williams, C.R., 1995. Developments in UHF lower tropospheric wind profiling at NOAA's Aeronomy Laboratory. Radio Sci. 30, 977–1001.
Chakravarty, K., Maitra, A., 2010. Rain attenuation studies over an earth space path at a tropical location. J. Atmos. Sol. Terr. Phys. 72, 135–138.
Chakravarty, K., Raj, P.E., 2013. Raindrop size distributions and their association with characteristics of clouds and precipitation during monsoon and post-monsoon periods over a tropical Indian station. Atmos. Res. 124, 181–189.
Chakravarty, K., Raj, P.E., Bhattacharya, A., Maitra, A., 2013. Microphysical characteristics of clouds and precipitation during pre-monsoon and monsoon period over a tropical Indian station. J. Atmos. Sol. Terr. Phys. 94, 28–33.
Chapon, B., Delrieu, G., Gosset, M., Boudevillain, B., 2008. Variability of rain drop size distribution and its effect on the Z–R relationship: a case study for intense Mediterranean rainfall. Atmos. Res. 87, 52–65.
Chen, B., Yang, J., Pu, J., 2013. Statistical characteristics of raindrop size distribution in the meiyu season observed in Eastern China. J. Meteorol. Soc. Japan. 91 (2), 215–227.
Cohen, C., Mc Caul Jr, E.W., 2006. The sensitivity of simulated convective storms to variations in prescribed single-moment microphysics parameters that describe particle distributions, sizes, and numbers. Mon. Weather Rev. 134, 2547–2565.
Curic, M., Janc, D., Veljovic, K., 2010. Dependence of accumulated precipitation on cloud drop size distribution. Theor. Appl. Climatol. 102, 471–481.
Das, S., Maitra, A., Shukla, A.K., 2010. Rain attenuation modeling in the 10–100 GHz frequency using drop size distributions for different climate zones in tropical India. Prog. Electromagn. Res. B 25, 211–224.
Ecklund, W.L., Carter, D.A., Balsley, B.B., 1988. A UHF wind profiler for the boundary layer: brief description and initial results. J. Atmos. Ocean. Technol. 5, 432–441.
Fabry, F., Zawadzki, I., 1995. Long-term radar observations of the melting layer of precipitation and their interpretation. J. Atmos. Sci. 52, 838–851.
Friedrich, Katja, Evan, A. Kalina, Forrest, J.Masters, Carlos, R. Lopez, 2013. Drop size distributions in thunderstorms measured by optical disdrometers during VORTEX2. Mon. Weather Rev. 141, 1182–1203.
Gilmore, M.S., Straka, J.M., Rasmussen, E.N., 2004b. Precipitation uncertainty due to variations in precipitation particle parameters with in a simple microphysics scheme. Mon. Weather Rev. 132, 2610–2627.
Gossard, E.E., Strauch, R.G., Rogers, R.R., 1990. Evolution of drop size distribution in liquid precipitation observed by ground-based Doppler radar. J. Atmos. Ocean. Technol. 7, 815–828.

Gunn, R., Kinzer, G.D., 1949. The terminal velocity of fall for water droplets in stagnant air. J. Meteorol. 6, 233–248.
Hu, Z., Srivastava, R.C., 1995. Evolution of raindrop size distribution by coalescence, breakup, and evaporation: theory and observation. J. Atmos. Sci. 52, 1761–1783.
Iguchi, T., Kozu, T., Meneghine, R., Awaka, J., Okamoto, K., 2000. Rain-profiling algorithm for the TRMM precipitation radar. J. Appl. Meteorol. 39, 2038–2052.
Jayalakshmi, J., Reddy, K.K., 2014. Raindrop size distributions of south west and north east monsoon heavy precipitations observed over Kadapa (14° 4′ N, 78° 82′ E), a semi-arid region of India. Curr. Sci. 107 (8), 1312–1320.
Joss, J., Waldvogel, A., 1969. Raindrop size distribution and sampling size errors. J. Atmos. Sci. 26, 566–569.
King, M.D., Menzel, W.P., Kaufman, Y.J., Tanre, D., Gao, B.-C., Platnick, S., Ackerman, S.A., Remer, L.A., Pincus, R., Hubanks, P.A., 2003. Cloud and aerosol properties, precipitable water, and profiles of temperature and water vapor. IEEE Trans. Geosci. Remote Sens. 41, 442–458.
Kozu, T., Shimomai, T., Akramin, Z., Marzuki, Shibagaki Y., Hashiguchi, H., 2005. Intraseasonal variation of raindrop size distribution at Koto Tabang,West Sumatra, Indonesia. Geophys. Res. Lett. 32, L07803. http://dx.doi.org/10.1029/2004GL022340.
Kozu, T., Reddy, K.K., Mori, S., Thurai, M., Ong, J.T., Rao, D.N., Shimomai, T., 2006. Seasonal and diurnal variations of raindrop size distribution in Asian monsoon region. *J. meteor*ol. Soc. Japan. 84 (A), 195–209.
Kozu, T., Masuzawa, K., Shimomai, T., Kashiwagi, N., 2010. Estimation of N_0^* for the two-scale gamma raindrop size distribution model and its statistical properties at several locations in Asia. J. Appl. Meteorol. Climatol. 49, 676–686.
Krishna, U.V.M., Reddy, K.K., Mastanaiah, R., Shirooka, R., Pan, C.J., 2014. Observational study on melting layer characteristics over Palau in Pacific Ocean. J. Atmos. Sol. Terr. Phys. 121, 132–140.
Kubota, H., Shirooka, R., Ushiyama, T., Chuda, T., Iwasaki, S., Takeuchi, K., 2005. Seasonal variations of precipitation properties associated with the monsoon over Palau in the Western Pacific. J. Hydrometeorol. 6, 518–531.
Kummerow, C. Hong, Olson, W.S., Yang, S., Adler, R.F., McCollum, J., Ferraro, R., Petty, G., Shin, D.B., Wilheit, T.T., 2001. The evolution of the Goddard profiling algorithm (GPROF) for rainfall estimation from passive microwave sensors. J. Appl. Meteorol. 40, 1801–1840.
Maki, M., Keenan, T.D., Sasaki, Y., Nakamura, K., 2001. Characteristics of the raindrop size distribution in tropical continental squall lines observed in Darwin, Australia. J. Appl. Meteorol. 40, 1393–1412.
Marzuki, Kozu T., Shimomai, T., Hashiguchic, H., Randeua, W.L., Vonnisa, M., 2010. Raindrop size distributions of convective rain over equatorial Indonesia during the first CPEA campaign. Atmos. Res. 96, 645–655.
Marzuki, Randeu W.L., Kozu, T., Shimomai, T., Hashiguchi, H., Schönhuber, M., 2013. Raindrop axis ratios, fall velocities and size distribution over Sumatra from 2D-video disdrometer measurement. Atmos. Res. 119, 23–37.
Marzuki, Hashiguchi, Hiroyuki, Kozu, Toshiaki, Shimomai, Toyoshi, Shibagaki, Yoshiaki, Takahashi Yukihiro, 2016. Precipitation microstructure in different Madden–Julian Oscillation phases over Sumatra. Atmos. Res. 168, 121–138.
Moteki, Q., Shirooka, R., Kubota, H., Ushiyama, T., Reddy, K.K., Yoneyama, K., Katsumata, M., Sato, N., Yasunaga, K., Yamada, H., Geng, B., Fujita, M., Masanori, Y., Uyeda, H., Chuda, T., 2008. Mechanism of the northward propagation of mesoscale convective systems observed on 15 June 2005 during PALAU 2005. J. Geophys. Res. 113 (doi: 10.1029/Res.,D141262008JD009793).
Nakajima, T., King, M.D., 1990. Determination of the optical thickness and effective particle radius of clouds from reflected solar radiation measurements, part I: theory. J. Atmos. Sci. 47, 1878–1893.
Niu, Shengjie, Jia, Xingcan, Sang, Jianren, Liu, Xiaoli, Lu, Chunsong, Liu, Yangang, 2010. Distributions of raindrop sizes and fall velocities in a semiarid plateau climate: convective versus stratiform rains. J. Appl. Meteorol. Climatol. 49, 632–645.
Platnick, S., King, M.D., Ackerman, S.A., Menzel, W.P., Baum, B.A., Riedl, J.C., Frey, R.A., 2003. The MODIS cloud products: algorithms and examples from Terra. IEEE Trans. Geosci. Remote Sens. 41, 459–473.
Rao, T.N., Rao, D.N., Mohan, K., Raghavan, S., 2001. Classification of tropical precipitating systems and associated Z–R relationships. J. Geophys. Res. 106, 17699–17711.
Rao, T.N., Radhakrishna, B., Nakamura, K., Rao, N.P., 2009. Differences in raindrop size distribution from southwest monsoon to northeast monsoon at Gadanki. Q. J. R. Meteorol. Soc. 135, 1630–1637.
Reddy, K.K., Kozu, T., 2003. Measurements of raindrop size distribution over Gadanki during southwest and northeast monsoon. Indian J. Radio Space Phys. 32, 286–295.
Reddy, K.K., Kozu, T., Ohno, Y., Jain, A.R., Rao, D.N., 2005. Estimation of vertical profiles of raindrop size distribution from the VHF wind profiler radar Doppler spectra. Indian J. Radio Space Phys. 34, 319–327.
Remer, L.A., Kaufman, Y.J., Tanré, D., Mattoo, S., Chu, D.A., Martins, J.V., Li, R.-R., Ichoku, C., Levy, R.C., Kleidman, R.G., Eck, T.F., Vermote, E., Holben, B.N., 2005. The MODIS aerosol algorithm, products, and validation. J. Atmos. Sci. 62, 947–973.
Rosenfeld, D., Ulbrich, C.W., 2003. Cloud microphysical properties, processes, and rainfall estimation opportunities. Meteorol. Monogr. 30 (52), 237–258.
Schönhuber, M., Lammer, G., Randeu, W.L., 2008. The 2D-Video-Distrometer, Chapter 1. In: Michaelides, Silas (Ed.), Precipitation: Advances in Measurement, Estimation and Prediction. Springer. ISBN: 978-3-540-77654-3.
Sharma, S., Konwar, M., Sarma, D., Kalapureddy, M., Jain, A.R., 2009. Characteristics of rain integral parameters during tropical convective, transition and stratiform rain at Gadanki and its application in rain retrieval. J. Appl. Meteorol. Climatol. 48, 1245–1266.
Sheppard, B.E., Joe, P.I., 1994. Comparison of raindrop size distribution measurements by a Joss–Waldvogel disdrometer, a PMS 2DG Spectrometer, and a POSS Doppler radar. J. Atmos. Ocean. Technol. 11, 874–887.
Steiner, M., Waldvogel, A., 1987. Peaks in raindrop size distributions. J. Atmos. Sci. 44, 3127–3133.
Steiner, M., Houze, R.A., Yuter, S.E., 1995. Climatological characterization of 3-dimensional storm structure from operational radar and rain-gauge data. J. Appl. Meteorol. 34, 1978–2007.
Steiner, M., Smith, J.A., Uijlenhoet, R., 2004. A microphysical interpretation of radar reflectivity rainrate relationships. J. Atmos. Sci. 61, 1114–1131.
Suh, S.-H., You, C.-H., Lee, D.-I., 2015. Climatological characteristics of raindrop size distributions within a topographically complex area. Hydrol. Earth Syst. Sci. Discuss. 12, 4005–4045. http://dx.doi.org/10.5194/hessd-12-4005-2015.
Testud, J., Oury, S., Amayenc, P., Black, R.A., 2001. The concept of "normalized" distributions to describe raindrop spectra: a tool for cloud physics and cloud remote sensing. J. Appl. Meteorol. 40, 1118–1140.
Thurai, M., Gatlin, P.N., Bringi, V.N., 2016. Separating stratiform and convective rain types based on the drop size distribution characteristics using 2D video disdrometer data. Atmos. Res. 169, (Part B), 416–423.
Tokay, A., Short, D.A., 1996. Evidence from tropical raindrop spectra of the origin of rain from stratiform versus convective clouds. J. Appl. Meteorol. 35, 355–371.
Tokay, A., Kruger, A., Krajewski, W.F., 2001. Comparison of drop size distribution measurements by impact and optical disdrometers. J. Appl. Meteorol. 40, 2083–2097.
Tokay, A., Kruger, A., Krajewski, W.F., Kucera, P.A., FilhoA, J.P., 2002. Measurements of drop size distribution in the southwestern Amazon basin. J. Geophys. Res. 107 (D20), 8052. http://dx.doi.org/10.1029/2001JD000355.
Tokay, A., Wolff, David B., Wolff, Katherine R., Bashor, Paul, 2003. Rain gauge and disdrometer measurements during the Keys Area Microphysics Project (KAMP). J. Atmos. Ocean. Technol. 20, 1460–1477.
Tokay, A., Bashore, P.G., Habib, E., Kaqspari, T., 2008. Raindrop size distribution measurements in tropical cyclones. Mon. Wea. Rev. 136, 1669–1685.
Tokay, A., Petersen, Walter A., Gatlin, Patrick, Wingo, Matthew, 2013. Comparison of raindrop size distribution measurements by collocated disdrometers. J. Atmos. Ocean. Technol. 30, 1672–1690.
Ulbrich, C.W., 1983. Natural variations in the analytical form of the raindrop size distribution. J. Clim. Appl. Meteorol. 22, 1764–1775.
Ulbrich, C.W., Atlas, D., 2007. Microphysics of raindrop size spectra: tropical continental and maritime storms. J. Appl. Meteorol. Climatol. 46, 1777–1791.
Ushiyama, T., Reddy, K.K., Kubota, H., Yasunaga, K., Shirooka, R., 2009. Diurnal to inter annual variation in the raindrop size distribution over Palau in the western tropical Pacific. Geophys. Res. Lett. 36, L02810. http://dx.doi.org/10.1029/2008GL036242.
van den Heever, S.C., Cotton, W.R., 2004. The impact of hail size on simulated supercell storms. J. Atmos. Sci. 61, 1596–1609.
Waldvogel, A., 1974. The N_0 jump of raindrop spectra. J. Atmos. Sci. 31, 1067–1978.
Williams, C.R., Ecklund, W.L., Gage, K.S., 1995. Classification of precipitating clouds in the tropics using 915-MHz wind profilers. J. Atmos. Ocean. Technol. 12, 996–1011.
Zawadzki, I., Fabry, F., Szyrmer, W., 2001. Observations of super cooled water and secondary ice generation by a vertically pointing X-band Doppler radar. Atmos. Res. 59–60, 343–359.